DOI: 10.1002/chem.200903362

Photochemistry and Reactivity of the Phenyl Radical–Water System: A Matrix Isolation and Computational Study

Artur Mardyukov,[a] Rachel Crespo-Otero,[a] Elsa Sanchez-Garcia,[b] and Wolfram Sander*[a]

Dedicated to Professor Wolfgang Kirmse on the occasion of his 80th birthday

Abstract: The reaction of the phenyl radical **1** with water has been investigated by using matrix isolation spectroscopy and quantum chemical calculations. The primary thermal product of the reaction between **1** and water is a weakly bound complex stabilized by an OH···π interaction. This complex is photolabile, and visible-light irradiation ($\lambda > 420$ nm) results in hydrogen atom transfer from water to radical **1** and the formation of a highly labile complex between benzene and the OH radical. This complex is stable under the conditions of matrix isolation, however, continuous irradiation with $\lambda > 420$ nm light results in the complete destruction of the aromatic system and formation of an acylic unsaturated ketene. The mechanisms of all reaction steps are discussed in the light of ab initio and DFT calculations.

Keywords: density functional calculations · infrared spectroscopy · matrix isolation · photochemistry · radical reactions

Introduction

The phenyl radical (**1**) is a reactive intermediate of fundamental importance to organic chemistry. It has been shown to play a key role in the combustion of hydrocarbon fuels to produce polycyclic aromatic hydrocarbons and soot.[1] It has also been discussed as an intermediate in the chemistry of the interstellar medium, especially for the formation of polycyclic aromatic hydrocarbons,[2] and in tropospheric chemistry.[3,4] The most important reaction for the removal of benzene (**2**) from the troposphere is the reaction with the OH radical. For this reaction two channels have been observed in the gas phase: 1) hydrogen abstraction to give **1** and water and 2) addition to give 2-hydroxy-3,5-cyclohexadienyl (**3**) (Scheme 1). In the troposphere the sequence of reactions following the formation of radical **3** is fairly complex and not well understood.

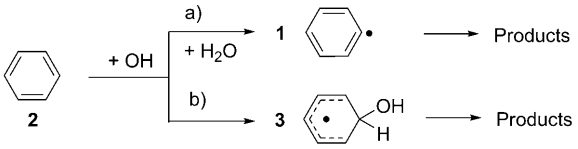

Scheme 1. Reaction channels for the reaction of **2** with OH in the gas phase.

Due to its great importance, the reaction between **2** and the OH radical has been the subject of a large number of experimental[5–11] and theoretical studies.[12–22] At higher temperatures (above room temperature) reaction channel a, producing **1** and water dominates, whereas at room temperature and below reaction channel b, the addition of OH to **2** to give **3**, is the major pathway. One of the products of this reaction channel is phenol.

In a computational study at the G3 level of theory Tokmakov and Lin investigated the mechanism of the **2**+OH reaction and found that channel a proceeded by a single-step reaction with an activation barrier of 5.3 kcal mol^{-1} and a reaction energy of −4.2 kcal mol^{-1}.[14] In contrast, the OH addition, channel b, proceeds via a prereaction complex **2**···OH. This complex shows a nonbonding interaction between the O atom and one of the C atoms of **2** and the OH hydrogen atom pointing in the direction of the π system of **2**. The complex is stabilized by 2.6 kcal mol^{-1}, which increas-

[a] A. Mardyukov, Dr. R. Crespo-Otero, Prof. Dr. W. Sander
Lehrstuhl für Organische Chemie II, Ruhr-Universität Bochum
44780 Bochum (Germany)
Fax: (+49) 234-321-4353
E-mail: wolfram.sander@rub.de

[b] Dr. E. Sanchez-Garcia
Max-Planck Institut für Kohlenforschung, Mülheim an der Ruhr
Kaiser-Wilhelm-Platz 1, 45470 Mülheim an der Ruhr (Germany)

Supporting information for this article is available on the WWW under http://dx.doi.org/10.1002/chem.200903362.

es the activation barrier for the addition of OH to **2** from 2.8 kcal mol^{-1} (relative to the separated reactants) to 5.4 kcal mol^{-1} (relative to the **2**···OH complex). The formation of prereactive complexes in radical reactions has recently been investigated by several authors.[23–26] It has been shown that carbon-centered radicals indeed can function as hydrogen-bond acceptors. However, due to the low electronegativity of carbon and since radicals provide only one electron and not two like atoms with lone pairs, the hydrogen bonds to carbon-centered radicals are quite weak.

In a combined experimental and theoretical study Platz et al. investigated solvent effects for the addition of OH to **2**.[8] By using laser flash photolysis it was shown that the addition in water is faster by a factor of 65 than in acetonitrile, which could not be explained by the differences in the dielectric constants of these two solvents. DFT calculations using the B3LYP functional revealed that the free energy of activation at room temperature for the hydrogen abstraction is about 1 kcal mol^{-1} higher than for the addition, and thus addition should predominate. In this study, a weakly bound complex (similar to that described by Tokmakov and Lin obtained with a slightly different basis set)[14] was used as a starting point for the reactions between **2** and OH for both reaction channels. At the B3LYP/6-311+G**//B3LYP/6-31+G** level of theory, a binding energy of the complex of −3.65 kcal mol^{-1} was calculated and ΔG was calculated to +3.96 kcal mol^{-1}. The solvent effect of the addition reaction was explained by the formation of specific complexes between solvent molecules and the OH radical. The reaction of OH complexed with water has a significantly lower activation barrier than that of OH complexed with acetonitrile.

In the temperature range between 325 and 380 K the gas-phase reaction between OH and **2** shows a nonlinear Arrhenius plot and the decay of OH is nonexponential. In a computational study by Alvarez-Idaboy et al., this complex kinetic behavior was explained by the competition between the addition reaction and hydrogen abstraction and by the reversibility of the addition reaction.[22] Thus, the decomposition of radical **3** back to **2** and OH is of importance to understand the experimental kinetic data.

Recently, we described the formation of a weakly bound complex between the phenyl radical **1** and water under the conditions of matrix isolation.[5] This complex proved to be photolabile, and with visible-light irradiation reacted to a complex between the hydroxyl radical and **2**. We now found that this second complex is also photolabile and irradiation surprisingly results in ring opening and formation of a highly unsaturated ketene. Herein we describe a detailed mechanistic and computational study on the reaction between **1** and water. The sequence of reactions starts with **1** interacting with water and ends with the complete destruction of the aromatic ring system under fairly mild irradiation conditions. A detailed knowledge of the elemental steps of this reaction sequence can contribute to the understanding of the highly complex processes involved in the combustion and degradation of aromatic compounds.

Results and Discussion

The water–phenyl radical complex: The phenyl radical (**1**) was generated by flash vacuum pyrolysis (FVP) of azobenzene **4** at 500 °C with subsequent trapping of the products in solid argon at 10 K (Scheme 2). A second major product

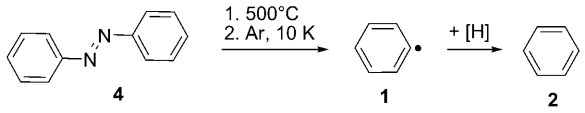

Scheme 2.

formed under these conditions is **2**, obtained from **1** either by hydrogen abstraction from surface contaminations of the pyrolysis oven or by bimolecular reactions or rearrangements in the gas phase. Since pyrolysis of the perdeuterated [D_{10}]**4** yields mainly [D_6]**2**, the main source of hydrogen comes from **4**. The IR spectrum of matrix-isolated **1** with the strongest absorptions at 705.8 and 657.4 cm^{-1} is in agreement with literature data.[27]

The advantage of generating **1** in the gas phase followed by trapping with excess argon is that, under these conditions, statistically most matrix cages contain only one molecule of **1**, whereas the photolysis of a matrix-isolated precursor produces radical pairs in the matrix cages. Annealing of matrices containing radical pairs results almost exclusively in radical recombination, whereas isolated radicals are able to undergo bimolecular reactions with added dopands. This has been shown previously in the case of O_2-doped argon matrices in which, at temperatures below 15 K, the diffusion of trapped molecules is very slow and no reaction between **1** and O_2 is observed. Annealing at 30 K, however, allows rapid diffusion of O_2 and the phenylperoxy radical is formed in a clean bimolecular reaction.[28]

Doping argon matrices containing the products of the FVP of **2** with 0.1–1 % of H_2O results in some significant changes in the IR spectra. Most notably are these changes in the area of the out-of-plane (o.o.p) CH deformation modes between 650 and 720 cm^{-1} (Figure 1). The strong fundamental ν_4 deformation of **2** (a_{2u} symmetrical o.o.p. C–H deformation mode, in-phase movement of all hydrogen

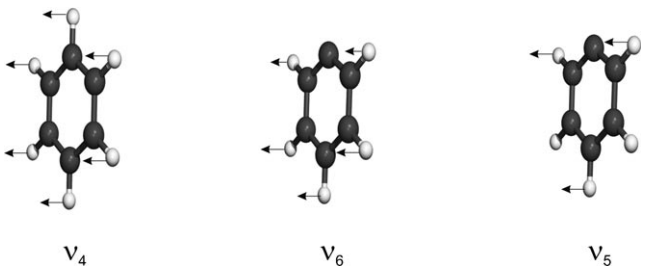

Figure 1. Displacement vectors showing some o.o.p. C–H deformation vibrations of **2** and **1**.

atoms) at 675.2 cm^{-1} is blueshifted by 6.8 cm^{-1} in the **2**···H_2O complex, in very good agreement with the observations of Engdahl and Nelander.[29] If the argon is doped with only 0.1% H_2O, this band is very weak after the deposition of the matrix at 10 K, but increases in intensity during annealing at temperatures above 25 K. In [D_6]**2** ν_4 shows a very large isotopic shift to 497.4 cm^{-1}, and the [D_6]**2**···H_2O complex shows a blueshift of 3.5 cm^{-1}. As expected, isotopic labeling of water (deuterium or ^{18}O) does not influence this vibration.

Matrix-isolated **1** shows strong IR bands at 705.8 (ν_6) and 657.4 cm^{-1} (ν_5), in good agreement with literature data.[27] After annealing a matrix containing **1** and 0.1% of H_2O for several minutes at 30 K, these bands decrease in intensity and new bands appear at 711.4 and 659.8 cm^{-1}. The blueshifts of 5.6 and 2.4 cm^{-1}, respectively, are similar to that of the corresponding bands in the **2**···H_2O complex (Figure 2).

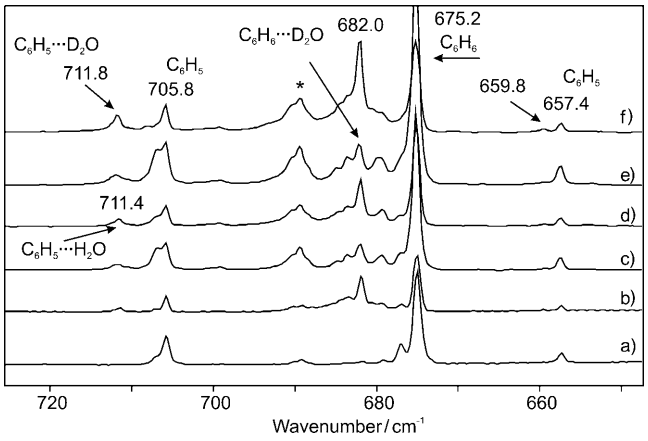

Figure 2. a) IR spectrum of a mixture of **1** and **2** in argon doped with 0.1% H_2O at 10 K, and b) after warming from 10 to 40 K with approximately 1 K min^{-1}. c) IR spectrum of a mixture of **1** and **2** in argon doped with 1% H_2O at 10 K, and d) after warming from 10 to 40 K with approximately 1 K min^{-1}. e) IR spectrum of a mixture of **1** and **2** in argon doped with 1% D_2O at 10 K, and f) after warming from 10 to 40 K with approximately 1 K min^{-1}. Bands of remaining azobenzene **4** are marked *.

The new bands appear only when both **1** and water are present in the matrix, and the band intensities increase if the concentration of one of the two monomers is increased (Figure 2d). We therefore assign these bands to the o.o.p. C–H deformation modes ν_6 and ν_5 of a **1**···H_2O complex. The bands of this complex already appear at low concentrations of water, which indicates that a 1:1 complex containing only one molecule of water is formed. If D_2O is used in these experiments, the o.o.p. vibrations of **1** in the complex show basically the same shifts as with H_2O (Figure 2d and f and Table 2). Other vibrations of **1** are not affected by the formation of the **1**···H_2O complex.

The o.o.p. C–D deformation mode ν_6 of [D_5]**1** is found at 518.0 cm^{-1} (Figure 3).[27] In the presence of H_2O, the formation of the [D_5]**1**···H_2O complex is indicated by a new band at 522.3 cm^{-1} that corresponds to a blueshift of 4.3 cm^{-1} with respect to the monomer.

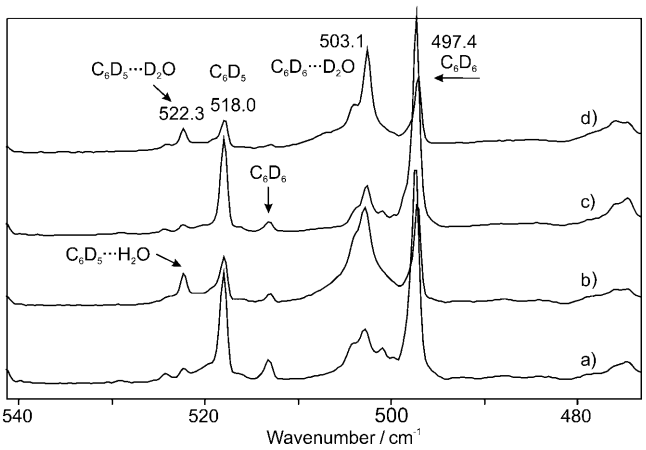

Figure 3. a) IR spectrum of a mixture of [D_5]**1** and [D_6]**2** in argon doped with 1% H_2O at 10 K, and b) after warming from 10 to 40 K with approximately 1 K min^{-1}. c) IR spectrum of a mixture of [D_5]**1** and [D_6]**2** in argon doped with 1% D_2O at 10 K, and d) after warming from 10 to 40 K with approximately 1 K min^{-1}.

Water is quite mobile in argon, and even at low temperature and at low concentrations some molecules are rotating and diffusion is rapid enough to easily form aggregates.[30–32] This results in complex IR patterns in the O–H stretching region, and therefore the assignment of bands of the **1**···H_2O complex in this spectral region is difficult. The ν_2 mode of the water monomer is observed at 3639.7 cm^{-1}.[30] The formation of **1**···H_2O results in a new band at 3618.0 cm^{-1}, which is redshifted by 21.7 cm^{-1} with respect to the monomer (Figure 1AS in the Supporting Information). As expected, deuteration of the phenyl radical in [D_5]**1**···H_2O does not influence this vibration (Table 2). The O–D stretching mode (ν_2) of **1**···D_2O is observed at 2645.1 cm^{-1}, redshifted by

Table 1. Calculated stabilization energies of C_6H_5···H_2O complexes [kcal mol^{-1}].

	UB3LYP[a]			UM05-2X[b]			RHF-UCCSD(T)[c]	
Complex	ΔE	ΔE_{CP}	ΔE_{CP+ZPE}	ΔE	ΔE_{CP}	ΔE_{CP+ZPE}	ΔE	ΔE_{CP}
A	−1.71	−1.44	−0.67	−3.77	−3.26	−2.38	−3.69	−2.45
B	–[d]	–	–	−3.01	−2.76	−1.68	−2.71	−1.77
BI	−2.00	−1.74	−0.79	−2.88[e]	–	–	–	–
C	–	–	–	−2.23	−2.04	−1.09	−2.38	−1.69
CI	−1.18	−1.02	−0.42	–	–	–	–	–
D	−1.09	−0.92	−0.27	−2.10	−1.91	−1.03	−2.27	−1.59
E	−1.11	−0.96	−0.37	−1.65[e]	–	–	–	–

[a] UB3LYP/6-311++G(2d,2p). [b] UM05-2X/6-311++G(2d,2p). [c] RHF-UCCSD(T)/6-311++G(2d,2p)//UM05-2X/6-311++G(2d,2p). [d] Optimization of **B** at the B3LYP level leads to **BI**. [e] At the M05-2X level **BI** is a transition state (TS) leading to **B** with one imaginary vibration at 25 cm^{-1}. [f] At the M05-2X level, E is a transition state (TS) leading to **D** with one imaginary vibration at 18 cm^{-1}.

13.4 cm^{-1} from ν_2 of D_2O at 2658.5 cm^{-1} (Figure 1BS in the Supporting Information).

The frequencies and the frequency shifts in the **1**···H_2O complex are similar to those of **2**···H_2O,[29] which suggests that both complexes have similar structures with the water molecule located on top of the aryl π system forming a weak OH···π hydrogen bond. On the other hand, the radical center in **1** could also act as a hydrogen-bond acceptor, which should lead to a second complex with an in-plane water molecule and a OH···C(radical) hydrogen bond. We therefore systematically investigated the interactions between **1** and water using DFT methods. Since dispersion is important to describe these weakly bound complexes, we used the M05-2X functional developed by Truhlar and Zhao[33,34] with a large 6-311++G(2d,2p) basis set. At this level of theory four **1**···H_2O complexes **A**–**D** were found (Figure 4) that are stabilized by the following intermolecular interactions:

1) OH···π interaction between one hydrogen atom of the water molecule and the π system of **1**; this can be regarded as a weak OH···π hydrogen bond.
2) OH···C(radical) interaction between one hydrogen atom of the water molecule and the radical center of **1**. This interaction can be regarded as a weak OH···C(radical) hydrogen bond.

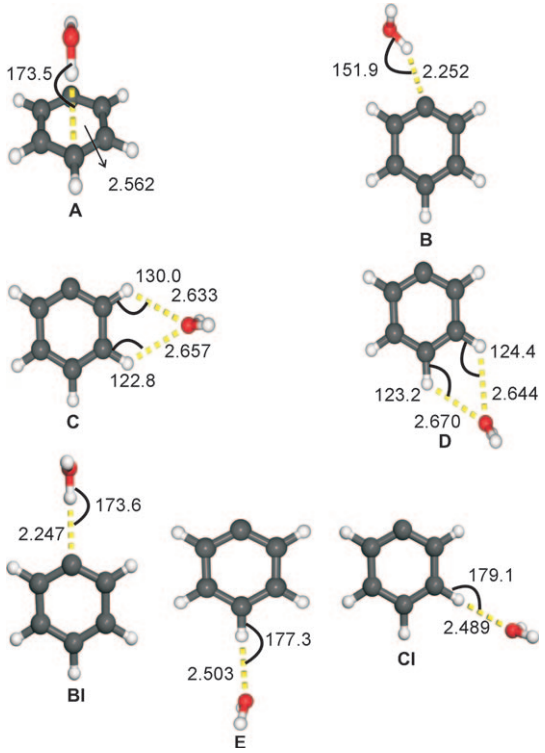

Figure 4. **1**···H_2O complexes **A**, **B**, **C**, and **D** calculated at the UM05-2X/6-311++G(2d,2p) level of theory. The complexes **B1**, **C1**, and **E** are no minima at this level and therefore the UB3LYP/6-311++G(2d,2p) geometries are presented herein. Hydrogen-bond lengths are shown in Å and angles in °.

Table 2. Experimental[a] and calculated (in italics)[b] IR spectroscopic data of the C_6H_5···H_2O complex.

	OH str.	CH o.o.p. def.	CH o.o.p. def.
H_2O	3639.4[c]		
	3894.2		
D_2O	2658.8[c]		
	2806.6		
$H_2{}^{18}O$	3630.7[e]		
	3886.1		
C_6H_5		705.8[d]	657.4[d]
		734.0	*681.8*
C_6D_5		518.0[d.]	–
		538.1	
C_6H_5···H_2O	3618.0 (−21.4)	711.4 (+5.6)	659.8 (+2.4)
A	*3863.5 (−30.7)*	*739.3 (+5.3)*	*682.6 (+0.8)*
B	*3806.2 (−88.0)*	*740.9 (+6.9)*	*680.5 (−1.3)*
C	*3887.7 (−6.5)*	*744.8 (+10.8)*	*684.1 (+2.3)*
D	*3887.8 (−6.4)*	*746.6 (+12.6)*	*684.6 (+2.8)*
C_6D_5···H_2O	3618.0 (−21.4)	522.3 (+4.3)	–
A	*3864.5 (−29.7)*	*540.2 (+2.1)*	–
B	*3806.2(−88.0)*	*539.1 (+1.0)*	–
C	*3887.7 (−6.5)*	*541.3 (+3.2)*	–
D	*3887.8 (−6.4)*	*544.5 (+6.4)*	–
C_6H_5···D_2O	2645.1 (−13.7)	711.8 (+6.0)	659.8 (+2.4)
A	*2787.1 (−19.5)*	*739.3 (+5.3)*	*682.6 (+0.8)*
B	*2862.0 (+56.0)*	*740.9 (+6.9)*	*680.4 (−1.4)*
C	*2801.7(−4.9)*	*744.7(+10.7)*	*684.1 (+2.3)*
D	*2801.8 (−4.8)*	*746.5 (+12.5)*	*684.5 (+2.7)*
C_6D_5···D_2O	2645.1 (−13.7)	522.3 (+4.3)	–
A	*2787.1 (−19.5)*	*539.9 (+1.8)*	–
B	*2862.0 (+55.4)*	*539.1 (+1.0)*	–
C	*2801.7 (−4.9)*	*541.2(+3.1)*	–
D	*2801.7 (−4.9)*	*544.3(+6.2)*	–
C_6H_5···$H_2{}^{18}O$	3610.5 (−20.2)	711.5 (+5.7)	659.5 (+2.1)
A	*3854.7 (−31.4)*	*739.3 (+5.3)*	*682.6 (+0.8)*
B	*3796.6 (−89.5)*	*740.9 (+6.9)*	*680.5 (+21.0)*
C	*3879.6 (−6.5)*	*744.8 (+10.8)*	*684.1(+2.3)*
D	*3879.7 (−6.4)*	*746.6 (+12.6)*	*684.6(+2.8)*

[a] Argon matrix. [b] M05-2X/6-311++G(2d,2p). [c] References [29,35,36]. [d] Reference [27]. [e] Reference [37].

3) CH···O interaction between one hydrogen atom of the phenyl radical and the oxygen atom of water. These are weak van der Waals interactions.

In both complexes **A** and **B**, radical **1** acts as a Lewis acid. While in **A** the π system acts as a hydrogen-bond acceptor, in **B** the unpaired electron is the acceptor. Complex **A** is the most stable complex (−2.39 kcal mol^{-1} CP and ZPE corrected) and is stabilized by interaction 1 between the OH group of water and the π system of **1** (Table 1). The UB3LYP and the UM05-2X calculated geometries of **A** are virtually identical.

The nonsymmetrical structure **B** follows in energy (−1.68 kcal mol^{-1}) and shows interaction 2 in which the OH group of the water molecule interacts with the radical center of **1**. The OHC angle is 151.9° and the hydrogen-bonding distance is 2.252 Å. When the B3LYP functional is used, the optimization of complex **B** leads to complex **BI**, with *Cs* symmetry, a hydrogen-bond distance of 2.247 Å, and an OHC hydrogen-bond angle 173.6° (Figure 4). With the M05-2X functional, the **BI** geometry is a transition state

(25i cm^{-1}) leading to **B**. This behavior is not surprising, since the potential energy surface of this kind of system is very flat. The B3LYP functional predicts **BI** as the most stable complex (-0.79 kcal mol^{-1}).

Much less stable than **A** and **B** are the *Cs* symmetrical complexes **C** and **D** (-1.09 and -1.03 kcal mol^{-1}, respectively) (Table 1). In these complexes, radical **1** acts as a Lewis acid through its C–H antibonding orbitals. They are both stabilized by interaction 2 and differ mostly in the position of the water molecule. In **C** the water molecule is located between the *ortho*- and *meta*-hydrogen atoms of **1**. In **D**, the water is found between the *meta*- and *para*-hydrogen atoms of **1**.

At the B3LYP level of theory, complexes **CI** and **E** are minima, whereas they are transition states with the M05-2X functional. The geometry optimization of **CI** and **E** using M05-2X leads to **C** and **D**, respectively (Figure 4). With B3LYP the interaction energies of all complexes after CP and ZPE corrections are below 1 kcal mol^{-1} and thus much smaller than at the M05-2X level. The differences in both geometries and energies indicate that the inclusion of dispersion energy is crucial for the correct description of the complexes.

The UM05-2X/6-311++G(2d,2p) vibrational frequencies of complex **A** are in good agreement with the experimental values (Table 2). Since the interactions in the complexes are very weak, the frequency shifts induced by complexation (compared with the monomers) are small. The largest shifts are found for the OH stretching mode of **B** (-88 cm^{-1}). In **A** the shift of the OH stretching mode is only -30.7 cm^{-1} (-26.4 cm^{-1} at the B3LYP/6-311++G(2d,2p) level of theory), which demonstrates that the stability of a hydrogen-bonded complex and the corresponding redshift of the X–H···Y vibration are not directly correlated.

In complex **B** the water molecule interacts directly with the unpaired electron of the radical, which results in a considerable spin transfer from **1** to the water molecule (Figure 5). Natural bond orbital (NBO) calculations indicate that the spin density on the water molecule is 0.02 e, mainly localized at the oxygen atom. This spin transfer in complex **B** results from the $n_C^{\sigma} \rightarrow \sigma^*_{O-H}$ donor–acceptor interaction, which contributes most to the stabilization of the complex. For the other complexes, the distribution of the spin densities does not differ significantly from the monomers. Their stabilization can be attributed to the $\pi_{C-C} \rightarrow \sigma^*_{O-H}$ (**A**) and $n_O^{\sigma} \rightarrow \sigma^*_{C-H}$ (**C** and **D**) interactions. These donor–acceptor interactions have similar contributions from the α and β orbitals, a behavior that has also been found in other radical–water complexes in which the radical acts as a Lewis acid.[23]

Hydroxyl radical–2 complex: Visible-light irradiation ($\lambda > 420$ nm) of an argon matrix containing the **1**···H_2O complex and the other products described above (mainly matrix isolated **1** and **2** and the **2**···H_2O complex) results in a rapid decrease of all IR absorptions assigned to **1**···H_2O, whereas other bands are not affected. During photolysis, new bands appear at 3502.2, 1482.8, 1040.3, and 684.2 cm^{-1} (Figure 6).

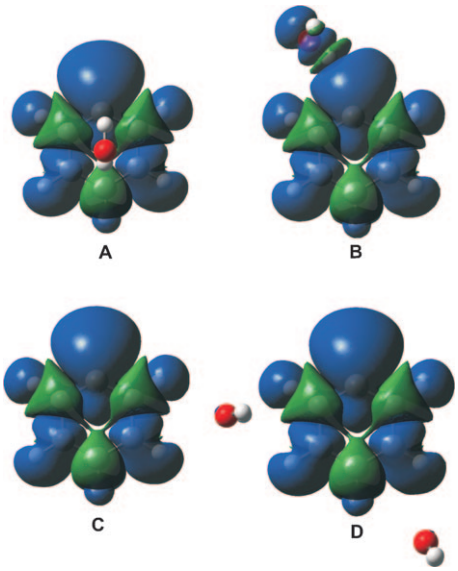

Figure 5. Spin densities in the **1**···H_2O complexes **A**–**D** calculated at the UM05-2X/6-311++G(2d,2p) level of theory.

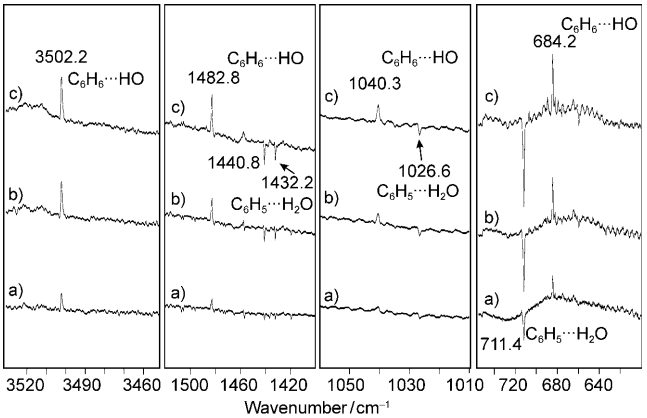

Figure 6. IR difference spectra showing the photochemical transformation of C_6H_5···H_2O into C_6H_6···HO. Bands pointing downwards assigned to C_6H_5···H_2O disappear and bands pointing upwards assigned to C_6H_6···HO appear after a) 1, b) 2, and c) 5 min irradiation at $\lambda > 420$ nm.

This selective photochemistry of **1**···H_2O allows for a detailed analysis of its photochemistry. To identify the photoproducts, five isotopomers of the complex have been investigated: **1**···H_2O, **1**···D_2O, **1**···$H_2{}^{18}O$, [D_5]**1**···H_2O, and [D_5]**1**···D_2O.

The bands at 1482.8 and 1040.3 are very close to the intense IR absorptions of matrix-isolated **2** at 1483 and 1041 cm^{-1},[29] whereas the band at 684.2 cm^{-1} is blueshifted from the very strong fundamental ν_4 of **2** at 675.2 cm^{-1} by 9 cm^{-1}. This indicates the formation of a complex of **2** similar to the **2**···H_2O complex. However, the 684.2 cm^{-1} band is clearly separated from the 682.0 cm^{-1} band of **2**···H_2O, which is also present in the matrix but not affected by the 420 nm irradiation.

If indeed **2** is formed during the photolysis of **1**···H_2O by hydrogen atom transfer from water to **1**, the other component of the complex of **2** has to be the hydroxyl radical (Scheme 3). The OH stretching vibration of the hydroxyl

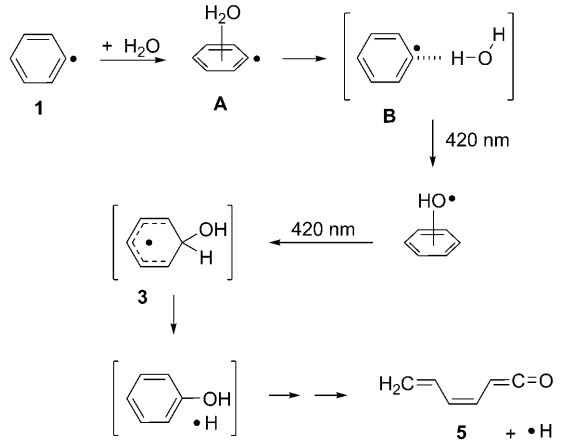

Scheme 3. Reaction of **1** with water.

radical in argon has been reported at 3548.2 cm^{-1}, the new band formed in this region during the photolysis of **1**···H_2O at 3502.2 cm^{-1} is redshifted from OH in argon by 46 cm^{-1}, which indicates the formation of a complex between the hydroxyl radical and **2**. Similar redshifts of the OH stretching mode of the hydroxyl radical have been reported in the literature.[38,39]

The formation of the **2**···HO complex is confirmed by isotopic labeling studies (Table 4) (Figure 2S in the Supporting Information):

1) If $H_2{}^{18}O$ is used in the experiments, the OH stretching vibration of the **2**···HO complex shows an isotopic shift of −11 cm^{-1}, in excellent agreement with that of OH in argon and clearly different from that of other OH-containing compounds (e.g., water or phenol). Other vibrations are not affected by ^{18}O isotopic substitution.
2) If D_2O is used, a deuterium atom is transferred to **1** and thus [D_1]**2** is formed. This results in a large deuterium isotopic shift of ν_4 of **2** from 684.2 in **2**···HO to 614.2 in [D_1]**2**···HO, in excellent agreement with the reported isotopic shifts in [D_1]**2**.[29] The OD vibration of the hydroxyl radical is now found at 2616.1 cm^{-1}, again in perfect agreement with the literature (Figure 2S in the Supporting Information).[39]
3) In a similar way, the photolysis of [D_5]**1**···H_2O results in the formation of [D_5]**2**···HO. These experiments clearly show the transfer of hydrogen or deuterium atoms from water to the phenyl radical.

The IR data of all isotopomers are summarized in Table 4.

The spectroscopic data were further confirmed by calculations of the **2**···HO complex using the UMP2, UM05-2X, and UB3LYP methods with the 6-311++G(2d,2p) basis set (Figure 7, Table 3). Very small spin contamination was found for the MP2 structure. Several starting geometries were used, however, no minima stabilized by CH···OH interactions were found, and the only minima that could be located are complexes with the OH···π interaction. With the UB3LYP method (very tight optimizations), the O atom of the hydroxyl radical is closer to the benzene ring than the H atom and interacting with one of the C atoms (Figure 7 **a**).[14,16] This structure is an intermediate towards the addition of OH to **2**. With UMP2 and UM05-2X, an OH···π complex is predicted with the H atom of the OH radical pointing towards the center of the π system (this complex was found with UB3LYP only when loose optimization cri-

Table 3. Stabilization energies for the C_6H_6···OH complex.

6-311++G(2d,2p)	ΔE	ΔE_{CP}	ΔE_{CP+ZPE}
UM05-2X	−4.71	−4.31	−3.08
UB3LYP	−3.41	−2.97	−1.71
UMP2	−4.50	−3.29	−2.80

Table 4. Experimental[a] and calculated (in italics)[b] IR spectroscopic data of the C_6H_6···OH complex.

	OH str.	Ring def.	Ring def.	CH o.o.p. def.
OH[c]	3548.2			
	3803.6			
OD[c]	2616.1			
	2769.1			
^{18}OH[c]	3537.1			
	3791.1			
C_6H_6[d]		1483.3	1041.2	675.0
		1546.9	*1081.4*	*698.0*
C_6D_6[d]		1334.7	816.3	497.2
		1395.4	*839.6*	*512.5*
C_6H_5D[d]		1480.2	1036.9	608.2
		1539.3	*1076.8*	*628.5*
C_6HD_5[e]		1392.6	818.3	922.3
		1344.1		513.2
C_6H_6···OH	3502.2 (−46)	1482.8 (−0.5)	1040.3 (−0.9)	684.2 (+9.2)
	3759.5 (−44.1)	1545.5 (−1.4)	1080.8 (−0.6)	711.7 (+13.7)
C_6HD_5···OH	3502.2 (−46)	1392.2 (−0.4)	818.8 (+0.5)	927.4 (+4.1)
		1343.3 (−0.8)		520.5 (+7.3)
C_6H_5D···OD	2583.4 (−32.7)	–	–	614.2 (+6.0)
C_6D_6···OD	2583.4 (−32.7)	–	816.6 (+0.3)	504.6 (+7.4)
	2737.1 (−32.0)	–	–	*521.6 (+9.1)*
C_6H_6···^{18}OH	3491.2 (−45.9)	1482.7 (−0.4)	1040.9 (−0.3)	684.2 (+9.2)
	3748.6 (−42.5)	*1545.1 (−1.8)*	*1080.6 (−0.8)*	*708.9 (+10.9)*

[c] Argon matrix. [d] UM05-2X/6-311++G(2d,2p). [e] Reference [40].

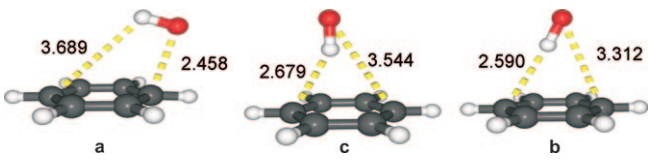

Figure 7. Geometry of the C_6H_6···HO complex calculated at several levels of theory. a) UB3LYP/6-311++G(2d,2p). b) UM05-2X/6-311++G(2d,2p). c) UMP2/6-311++G(2d,2p).

teria are used, which is not advisable for these types of systems) The UMP2 and UM05-2X OH···π complexes are calculated to be stabilized by −3.08 and −2.80 kcal mol^{-1} (including CP and ZPE corrections), respectively, whereas with UB3LYP the binding energy of the HO···C complex is only −1.71 kcal mol^{-1} (Table 3).

The frequencies calculated at the UM05-2X/6-311++G-(2d,2p) level of theory agree very well with the experimental IR data. In particular, the frequency shifts induced by the formation of the complex are nicely reproduced by the calculations. The largest frequency shift is observed for the OH stretching vibration with −46 cm^{-1}. With UM05-2X, UMP2 and UB3LYP the predicted shift is −44.1, −49.1 cm^{-1}, and +34.9 cm^{-1}, respectively, which clearly shows that B3LYP is not reliable to predict the structure of the complex.[41–43]

The transition state **a** shown in Figure 8 was located for the abstraction of a hydrogen atom from water by **1**. Intrinsic reaction coordinate (IRC) calculations using the B3LYP and M05-2X functionals confirm that this transition state directly connects the prereactive **1**···H_2O complex **B** with the the **2**···HO complex (Figure 8). The activation barrier for the hydrogen abstraction starting from complex **B** was calculated to 13.63 (9.84) kcal mol^{-1} with M05-2X (B3LYP). This barrier and the fact that the calculated ΔE of the reaction is 2.87 (3.53) kcal mol^{-1} with M05-2X (B3LYP) prevent a thermal reaction under the conditions of matrix isolation. Our experiments do not allow us to determine whether the hydrogen abstraction induced by visible-light irradiation proceeds on an excited-state surface and is thus a photochemical reaction or if the absorption of light just leads to vibrational excitation ("hot-ground-state" chemistry). The reverse reaction, the abstraction of a hydrogen atom from **2** by a hydroxyl radical has an activation barrier of 6.05 kcal mol^{-1} with respect to the isolated monomers and 10.76 kcal mol^{-1} (M05-2X functional) with respect to the **2**···HO complex.

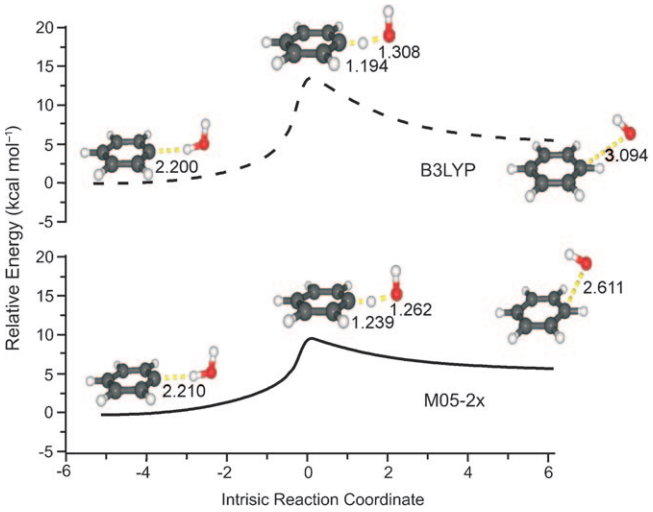

Figure 8. Intrinsic reaction coordinate (IRC) for the hydrogen transfer from water to **1**.

Photochemistry of the 2···HO complex: Prolonged visible-light irradiation ($\lambda > 420$ nm) of a matrix containing the **2**···HO complex results in bleaching of all bands of the complex and the appearance of a very strong band at 2130.8 cm^{-1} and several other new IR absorptions (Figure 9,

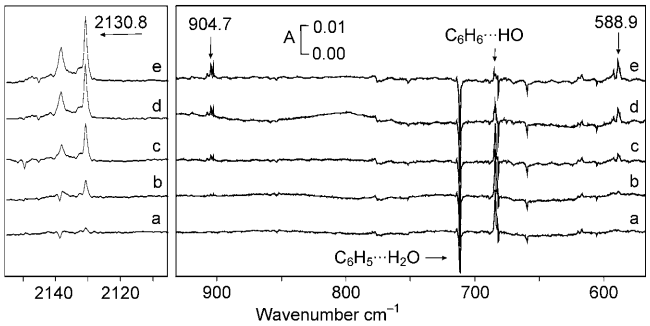

Figure 9. IR difference spectra showing the photochemistry of **1**···H_2O and **2**···HO during irradiation with $\lambda > 420$ nm in argon at 10 K. Bands pointing downwards assigned to **1**···H_2O disappear and bands pointing upwards assigned to ketene **5** appear after a) 1, b) 2, c) 5, d) 10, and e) 20 min irradiation time.

Table 5). The absorption at 2130.8 cm^{-1} is in the typical region of ketene C=C=O stretching vibrations. The use of $H_2{}^{18}O$ in the experiments results in a strong isotopic shift to

Table 5. IR spectroscopic data of the ring-opening product (Ar, 10 K).

C_6H_5···H_2O	C_6H_5···$H_2{}^{18}O$	C_6H_5···D_2O	C_6D_5···H_2O	C_6D_5···D_2O	Assignment
2130.8	2079.8	2130.7	2130.6	2130.7	ν(C=C=O)
1375.3	1375.2	1396.0			δ(C−H)
1373.5	1373.5				
904.7	904.6	747.2	736.2	727.7	ω(CH_2)
903.0	903.0				
592.4	592.4				ω(CH)
588.9	588.8				

2079.8 cm^{-1}, thus confirming the presence of a ketene group. Based on extensive isotopic labeling and comparison with DFT calculations, the newly formed compound is assigned to butadienylketene **5** (Scheme 3). Several configurations and conformations are possible for ketene **5**. However, due to the similarity of their calculated spectra a clear assignment of these geometrical isomers is not possible (Figure 3S in the Supporting Information).

Mechanism of the ketene formation: The mechanism for the formation of ketene **5** and a hydrogen atom by photolysis of the **2**···HO complex is not clear and requires a cascade of reaction steps. In the low-temperature experiments, no evidence for any intermediate was found for this reaction. However, since the formation of **5**, starting from azobenzene **4** and water, requires a long sequence of thermal and photochemical steps, the overall yield of **5** is low and we expect to observe intermediates only if they are formed in high stationary concentrations and if they contain strong IR chro-

mophores. A band that could not be assigned at 3409.4 cm^{-1} (shifted to 2509.8 cm^{-1} if D_2O was used) was formed as a by-product during the photolysis of **2**···HO. Products such as phenol could be ruled out by comparison with literature data and computed spectra.

Therefore, we undertook a detailed computational analysis to shed some light into the mechanism of the formation of **5** starting from radical **1**. Although it is not clear if this is a photochemical or a hot-ground-state reaction, only ground-state reactions were investigated. Four reaction channels were calculated at the B3LYP level of theory (Figure 10, Table 6 and Figures 9S and 10S in the Supporting Information). Only the more reasonable channels a and b are discussed herein, for the other two channels see the Supporting Information.

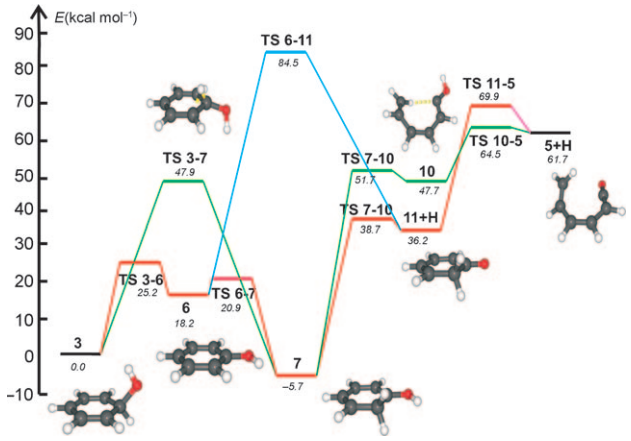

Figure 10. Energy profile [kcal mol^{-1}] of reaction channels a and b from radical **3** calculated at B3LYP/6-311++G(2d,2p) level of theory considering ZPVE.

Reaction channel a: The first and second reaction channels involve the formation of phenol **6** and a hydrogen atom as primary intermediates (Figure 10). The formation of **6** from radical **3** has been observed in the gas phase and is considered to be of importance to tropospheric chemistry (Scheme 4).[12,14] The barrier for the hydrogen loss is calculated to be 29.74 kcal mol^{-1} (25.20 kcal mol^{-1} considering ZPE corrections) using B3LYP/6-311++G(2d,2p) and 31.27 kcal mol^{-1} at the RHF-UCCSD(T)/6-311++G(2d,2p) level of theory.

A complex between **6** and a hydrogen atom stabilized by weak interactions was not found either with the B3LYP or with the M05-2X functional. Under the conditions of matrix isolation, we expect that the hydrogen atom is trapped in the host lattice in proximity to **6** and thus should be available for further reactions with **6**.

The calculated ΔE for the addition of a hydrogen atom to the *ortho* position of phenol **6** to produce radical **7** is 25.76 kcal mol^{-1}. The barrier for this reaction (**TS6-7**) is 1.63 kcal mol^{-1} at the B3LYP/6-311++G(2d,2p) level

Table 6. Relative energies of intermediates and transition states in the 3→5 reaction [kcal mol^{-1}].

	UB3LYP[a]		UCCSD(T)[b]
	E	E_{ZPE}	E
3	0	0	0
6+H	23.97	18.23	23.99
7	−5.39	−5.74	−3.83
11	42.87	36.24	41.24
5-ccc+H	70.34	61.70	71.19
10	49.73	47.73	52.84
12	28.28	28.14	28.32
13	15.86	13.84	20.40
14	50.13	47.93	52.14
TS3-6	29.74	25.20	31.27
TS6-7	25.60	20.86	27.57
TS7-10	44.57	38.79	46.64
TS11-5	78.62	69.95	81.06
TS7-10	51.73	49.45	54.74
TS10-5	72.11	64.47	75.23
TS3-12	49.53	46.65	51.21
TS12-13	39.72	37.56	41.46
TS13-5	81.84	73.83	89.04
TS3-7	50.78	47.14	53.55
TS3-14	57.61	55.04	58.00
TS12-13	51.18	46.91	57.54
TS6-11	94.73	84.75	97.37

[a] UB3LYP/6-311++G(2d,2p). [b] RHF-UCCSD(T)/6-311++G(2d,2p)//UB3LYP/6-311++G(2d,2p).

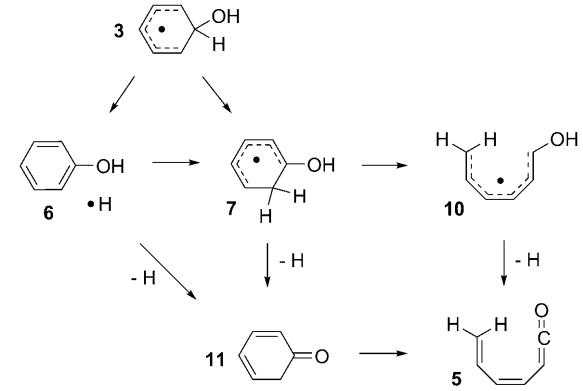

Scheme 4.

(2.63 kcal mol^{-1} with ZPE) and 3.58 kcal mol^{-1} at the RHF-UCCSD(T)/6-311++G(2d,2p) level of theory. Radical **7** is more stable than radical **3** by 5.74 kcal mol^{-1}.

The products of the addition of hydrogen to the *meta* and *para* positions of **6** are radicals **8** and **9**, respectively, which are 4.34 and 3.99 kcal mol^{-1}, respectively, more stable than **3**. The corresponding barriers are slightly larger than that obtained for the *ortho* addition: **TS6-8** 2.66 kcal mol^{-1} (3.65 kcal mol^{-1} including ZPE) for the *meta* addition, and **TS6-9** 2.23 kcal mol^{-1} (3.29 kcal mol^{-1} including ZPE) for the *para* addition. Therefore, the next steps are starting from the *ortho* radical **7**, although for **8** and **9** also pathways to **5** can be found.

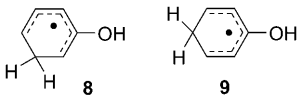

Radical **7** can also be formed in a single step from **3** via **TS3-7**. However, with a barrier of 49.96 kcal mol^{-1} (44.53 kcal mol^{-1} including ZPE, 50.53 kcal mol^{-1} at the RHF-CCSD(T)/6-311++G(2d,2p) level) the concerted reaction is much less favorable than the pathway via phenol **6** as an intermediate.

The tautomerism between phenol **6** and 2,4-cyclohexadienone (**11**) and the subsequent ring opening to form **5** is of importance for the mechanism of the reaction between **2** and OH in the gas phase and therefore has been much investigated.[44–47] The calculated barrier for the 1,3-H migration in **6** to give **11** via **TS6-11** is 70.76 kcal mol^{-1} (B3LYP, 66.52 kcal mol^{-1} including ZPE correction; 73.47 kcal mol^{-1} with RHF-UCCSD(T), in agreement with the value of 68.7 kcal mol^{-1} obtained by Xu and Lin at the G2//B3LYP/6-311G(d,p) level of theory.[47] The ring opening of **11** to **5** proceeds via **TS11-5** with a barrier of 35.75 kcal mol^{-1} (ZPE corrected: 33.69 kcal mol^{-1}; RHF-UCCSD(T): 40.82 kcal mol^{-1}).

Reaction channel b: This reaction path implies the ring opening of **7** to produce radical **10** via **TS7-10** (Figure 10). The barrier is 57.12 kcal mol^{-1} (ZPE corrected: 49.45 kcal mol^{-1}, RHF-UCCSD(T): 54.71 kcal mol^{-1}). The C–C distance (2.451 Å) is larger in **TS7-10** than in **TS11-5**. The barrier from **10** to **5** is 22.38 kcal mol^{-1} with the B3LYP functional (ZPE corrected: 16.74 kcal mol^{-1}) and 22.39 kcal mol^{-1} with RHF-UCCSD(T). The structure of **TS10-5** is similar to those of the final product **5** (Figures 4S and 6S in the Supporting Information).

In all reactions discussed above, ketene **5** is formed in the *cis*-configuration, *s-cis* conformation **5-ccc** (Figure 4S in the Supporting Information). The rotations around all bonds in **5** were considered and 8 isomers were found (Figure 7S in the Supporting Information). The most stable isomer is the *trans*-configuration, *anti*- conformation for all bonds (**5-ttt**). The isomer next in energy is **5-tct** (1.27 kcal mol^{-1}), which differs from **5-ttt** in the configuration of the central bond. The barriers for the rotation around the bonds with the larger single bond character in the **5-ccc** isomer to produce **5-cct** and **5-tcc** are 11.9 and 8.9 kcal mol^{-1}, respectively. The barriers from **5-cct** and **5-tcc** to produce the **5-tct** isomer are 4.0 and 3.7 kcal mol^{-1}. The rotation around the bond with the larger double character in **5-tct** has a barrier of 65.5 kcal mol^{-1} to produce the most stable isomer **5-ttt**. The spectra of all isomers are very similar (Table 7), therefore, an unambiguous assignment is not possible.

Table 7. Calculated relative energies (E_{rel}) and IR frequencies for the ring opening product at B3LYP/6-311++G(2d,2p) level of theory.

Isomers	E_{rel} [kcal mol^{-1}]	Vibrational mode [cm^{-1}]			
		ν(C=C=O)	δ(C–H)	ω(CH_2)	ω(CH)
5-ccc	7.56	2173.6	1443.7	955.5	562.2
5-cct	4.89	2182.1	1456.0	940.1	610.8
5-tcc	3.43	2170.5	1432.8	929.2	567.9
5-tct	1.27	2183.4	1418.4	926.3	609.1
5-ctc	5.41	2176.8	1424.3	927.1	655.8
5-ctt	3.63	2181.7	1429.4	925.5	606.4
5-ttc	1.75	2176.6	1425.9	916.6	579.2
5-ttt	0.00	2182.5	1399.1	916.7	615.2

Conclusion

Radical **1** and water easily form a weakly bound π complex **1**···H_2O, with a structure **A** similar to that of the complex between **2** and water. A second slightly less stable, according to our calculations, complex **B** with a hydrogen bond to the radical center is not observed in the experiments. However, complex **B** is the prereactive complex leading to the abstraction of a hydrogen atom from water. The activation barriers for the rearrangements **A**→**B** and **B**→**A** have to be smaller than the binding energy of **A** and **B**, respectively, which explains that even under the conditions of matrix isolation only the most stable complex is observed. On the other hand, complex **B** should be easily available upon thermal or photochemical excitation of **A**.

According to intrinsic reaction coordinate (IRC) calculations, complex **B** is directly connected to the **2**···HO complex. The activation barrier of 13.63 (9.84) kcal mol^{-1} at the M05-2X (B3LYP) level of theory is too high for a thermal reaction under the conditions of matrix isolation, however, visible-light irradiation completely drives the reaction to the **2**···HO complex. This reaction is slightly endothermic, but at room temperature calculated to be exergonic.[8] Our experiments do not allow us to differentiate between a photochemical reaction and a hot-ground-state reaction. It is most remarkable that the elusive complex between OH and **2** could be isolated and spectroscopically characterized, although it exists in a very shallow minimum only and is both thermo- and photolabile.

The structure calculated for the **2**···HO complex depends much on the theoretical method used for the calculation. At the B3LYP level of theory, the structure is that of **a** shown in Figure 7, in accordance with previous calculations.[8,14] This structure corresponds to an intermediate to the addition of OH to **2** with the O atom interacting with one of the ring carbon atoms. The hydrogen atom of OH only weakly interacts with the π system of **2**. In contrast, the structures obtained at the UM05-2X or UMP2 levels of theory show a strong OH···π interaction as in the **2**···H_2O complex. The stabilization energy calculated with these methods is considerably higher than that calculated with B3LYP. It is therefore plausible to assume that the B3LYP calculated structure is an artifact. This is confirmed by the comparison of the experimental IR spectrum of **2**···OH with the calculated spec-

tra. The B3LYP calculations predict a blueshift of the OH stretching vibration, which is in accordance with a C···O interaction and the OH hydrogen atom not involved in hydrogen bonding. In contrast, the UM05-2X and UMP2 calculations predict a redshift, as expected for the OH···π interaction, in excellent agreement with the experiment.

Irradiation of the **2**···HO complex leads directly to ketene **5** as the major product, whereas radical **3** or other intermediates are not observed. Radical **3** is the only plausible product formed from the **2**···HO complex, and all reasonable mechanisms for the formation of **5** require the formation of **3** as an intermediate. We therefore conclude that **3** is indeed formed, however, either with a large excess energy that leads to further reactions or it is photochemically unstable under the conditions of its formation. The formation of **5** and a hydrogen atom from radical **3** is calculated to be exothermic by 61.7 kcal mol^{-1}. If we assume that the hydrogen atom dimerizes to give molecular hydrogen, this value is reduced by 52 kcal mol^{-1}.

The most plausible reaction mechanism for the formation of ketene **5** is the sequence **3**→**6**+H→**7**→**11**+H→**5**+H. In the first step, phenol (**6**) and a hydrogen atom is formed from radical **3**. The hydrogen atom adds to the *ortho* position of **6** to give radical **7**. This loses the OH hydrogen atom to give **11**, which finally ring opens to **5**. Since we do not see any of the proposed intermediates experimentally, and we do not even know if the reaction proceeds in the ground state or an excited state, the mechanism remains speculative.

The reaction between **1** and water is highly efficient and allows us to observe several reactive intermediates, for the first time, that had been previously proposed in the degradation of **2**. The reaction between **1** and water presented herein allows us to gain insight into both reaction channels of the reaction between **2** and the OH radical: the hydrogen abstraction, coming from the product side, and the addition, resulting in the complete destruction of the aromatic ring system.

Experimental Section

Matrix isolation: The complexes between **1** and water were generated by codeposition of **1** and water with a large excess of argon at 10 K. In highly diluted matrices mainly the monomers were observed by IR spectroscopy. The monomers were easily identified by comparison with the data from the literature and with pure samples of matrix-isolated **1**[27,48] and water.[30,49,50] Water shows a high tendency for aggregation even in low-temperature matrices. These aggregates have been extensively studied by IR spectroscopy.[31,32,51] Matrices with higher concentrations of both **1** and water show IR absorptions that are not found in matrices containing only one of these components. These absorptions are thus assigned to mixed complexes between **1** and water. By annealing the argon matrices containing **1** and water at temperatures above 25 K, the small trapped molecules were allowed to diffuse, which results in an increase of the amount of aggregates. The dilution experiments in addition allowed differentiating the dimers from higher aggregates.

Computations: The multiple minima hypersurface (MMH) approach[52,53] was used to localize the minima for the **1**–water system. One thousand randomly arranged **1**–water dimers were generated as starting points in each case, and the PM3 and AM1[54,55] semiempirical Hamiltonians were used for the geometry optimizations. The most relevant minima were taken for further optimizations at higher levels of theory.

The DFT computations were performed by using the Gaussian 03 program.[56] The equilibrium geometries and vibrational frequencies were initially calculated with the B3LYP functional.[57,58] Since the complexes investigated herein are only weakly interacting and the OH···π interactions might play an important role, the hybrid *meta*-exchange correlation functional M05-2X,[59] which performs very well for noncovalent and weak interactions,[43,60–62] was also used. The Pople's triple ζ basis set augmented with diffuse and polarization functions 6-311++G(2d,2p) was employed.[63] All interaction energies were corrected for the BSSE by using the counterpoise (CP) method developed by Boys and Bernardi.[64] The stabilization energies were calculated by subtracting the energies of the monomers from those of the complexes including ZPE corrections.

All complexes were calculated at the unrestricted level of theory. Since the potential energy surface in the vicinity of the minima of the complexes is very flat, the very tight convergence criterion was used for the geometry optimizations.

Single-point RHF-UCCSD(T) calculations[65] for all complexes in the UM05-2X/6-311++G(2d,2p) geometries were performed by using the MOLPRO program.[66] For studying the reaction mechanisms, the geometries of reactants, products, intermediates, and transition states were optimized at the UB3LYP/6-311++G(2d,2p) level of theory. Harmonic frequencies were calculated in all cases. The energies were ZPE corrected, too. The transition states were identified as saddle points on the potential energies surfaces. A tight convergence criterion was used for all calculations. IRCs were calculated to confirm the connection between stationary points.[67] Single-point RHF-UCCSD(T) calculations of all structures were performed by using the UB3LYP/6-311++G(2d,2p) geometries. The NBO analysis was performed by using NBO3.[68]

Acknowledgements

This work was financially supported by the Deutsche Forschungsgemeinschaft (Forschergruppe 618) and the Fonds der Chemischen Industrie.

[1] Y. Li, L. Zhang, Z. Tian, T. Yuan, J. Wang, B. Yang, F. Qi, *Energy Fuels* **2009**, *23*, 1473–1485.
[2] R. J. McMahon, M. C. McCarthy, C. A. Gottlieb, J. B. Dudek, J. F. Stanton, P. Thaddeus, *Astrophys. J.* **2003**, *590*, L61L64.
[3] G. Ghigo, G. Tonachini, *J. Am. Chem. Soc.* **1998**, *120*, 6753–6757.
[4] R. Volkamer, B. Klotz, I. Barnes, T. Imamura, K. Wirtz, N. Washida, K. H. Becker, U. Platt, *Phys. Chem. Chem. Phys.* **2002**, *4*, 1598–1610.
[5] A. Mardyukov, E. Sanchez-Garcia, R. Crespo-Otero, W. Sander, *Angew. Chem.* **2009**, *121*, 4898–4901; *Angew. Chem. Int. Ed.* **2009**, *48*, 4804–4807.
[6] T. Seta, M. Nakajima, A. Miyoshi, *J. Phys. Chem. A* **2006**, *110*, 5081–5090.
[7] T. Berndt, O. Boege, *Phys. Chem. Chem. Phys.* **2006**, *8*, 1205–1214.
[8] M. P. DeMatteo, J. S. Poole, X. Shi, R. Sachdeva, P. G. Hatcher, C. M. Hadad, M. S. Platz, *J. Am. Chem. Soc.* **2005**, *127*, 7094–7109.
[9] S. Raoult, M.-T. Rayez, J.-C. Rayez, R. Lesclaux, *Phys. Chem. Chem. Phys.* **2004**, *6*, 2245–2253.
[10] R. H. Schuler, G. Albarran, *Radiat. Phys. Chem.* **2002**, *64*, 189–195.
[11] D. Johnson, S. Raoult, M.-T. Rayez, J.-C. Rayez, R. Lesclaux, *Phys. Chem. Chem. Phys.* **2002**, *4*, 4678–4686.
[12] C.-C. Chen, J. W. Bozzelli, J. T. Farrell, *J. Phys. Chem. A* **2004**, *108*, 4632–4652.
[13] C.-C. Chen, J. W. Bozzelli, *Chem. Phys. Proc. Combust.* **2003**, *13*–16.
[14] I. V. Tokmakov, M. C. Lin, *J. Chem. Phys.* **2002**, *116–117*, 11309–11326.
[15] D. L. Baulch, C. J. Cobos, R. A. Cox, C. Esser, P. Frank, T. Just, J. A. Kerr, M. J. Pilling, J. Troe, R. W. Walker, J. Warnatz, *J. Phys. Chem. Ref. Data* **1992**, *21*, 411–734.

[16] C. C. Chen, J. W. Bozzelli, J. T. Farrell, *J. Chem. Phys.* **2004**, *120–121*, 4632–4652.
[17] F. P. Tully, A. R. Ravishankara, R. L. Thompson, J. M. Nicovich, R. C. Shah, N. M. Kreutter, P. H. Wine, *J. Phys. Chem.* **1981**, *85*, 2262–2269.
[18] T. J. Wallington, D. M. Neuman, M. J. Kurylo, *Int. J. Chem. Kinet.* **1987**, *19*, 725–739.
[19] S. C. Lin, T. C. Kuo, Y. P. Lee, *J. Chem. Phys.* **1994**, *101*, 2098–2105.
[20] J. A. Manion, R. Louw, *J. Phys. Chem.* **1990**, *94*, 4127–4134.
[21] T. H. Lay, J. W. Bozzelli, J. H. Seinfeld, *J. Phys. Chem.* **1996**, *100*, 6543–6554.
[22] V. H. Uc, J. R. Alvarez-Idaboy, A. Galano, A. Vivier-Bunge, *J. Phys. Chem. A* **2008**, *112*, 7608–7615.
[23] R. Crespo-Otero, E. Sanchez-Garcia, R. Suardiaz, L. A. Montero, W. Sander, *Chem. Phys.* **2008**, *353*, 193–201.
[24] X. An, H. Liu, Q. Li, B. Gong, J. Cheng, *J. Phys. Chem. A* **2008**, *112*, 5258–5263.
[25] H. Hernandez-Soto, F. Weinhold, J. S. Francisco, *J. Chem. Phys.* **2007**, *127*, 164102.
[26] J. M. Merritt, S. Rudic, R. E. Miller, *J. Chem. Phys.* **2006**, *124*, 084301.
[27] A. V. Friderichsen, J. G. Radziszewski, M. R. Nimlos, P. R. Winter, D. C. Dayton, D. E. David, G. B. Ellison, *J. Am. Chem. Soc.* **2001**, *123*, 1977–1988.
[28] A. Mardyukov, W. Sander, *Chem. Eur. J.* **2009**, *15*, 1462–1467.
[29] A. Engdahl, B. Nelander, *J. Phys. Chem.* **1985**, *89*, 2860–2864.
[30] G. P. Ayers, A. D. E. Pullin, *Spectrochim. Acta Part A* **1976**, *32*, 1641–1650.
[31] J. Ceponkus, G. Karlstroem, B. Nelander, *J. Chem. Phys.* **2005**, *122–123*, 7859–7864.
[32] A. Engdahl, B. Nelander, *J. Chem. Phys.* **1987**, *86*, 4831–4837.
[33] Y. Zhao, D. G. Truhlar, *Acc. Chem. Res.* **2008**, *41*, 157–167.
[34] Y. Zhao, D. G. Truhlar, *J. Phys. Chem. A* **2008**, *112*, 1095–1099.
[35] G. P. Ayers, A. D. E. Pullin, *Spectrochim. Acta Part A* **1976**, *32*, 1641–1650.
[36] G. P. Ayers, A. D. E. Pullin, *Spectrochim. Acta Part A* **1976**, *32*, 1629–1639.
[37] G. P. Ayers, A. D. E. Pullin, *Spectrochim. Acta Part A* **1976**, *32*, 1689–1693.
[38] A. Engdahl, G. Karlstrom, B. Nelander, *J. Chem. Phys.* **2003**, *118*, 7797–7802.
[39] A. Engdahl, B. Nelander, *J. Chem. Phys.* **2005**, *122*, 126101.
[40] L. H. P. Weldon, C. L. Wilson, *J. Chem. Soc.* **1946**, 235–239.
[41] L. F. Holroyd, T. van Mourik, *Chem. Phys. Lett.* **2007**, *442*, 42–46.
[42] R. Crespo-Otero, L. A. Montero, W. D. Stohrer, J. M. G. de La Vega, *J. Chem. Phys.* **2005**, *123*, 134107.
[43] Y. Zhao, D. G. Truhlar, *J. Chem. Theory Comput.* **2007**, *3*, 289–300.
[44] R. Cypres, B. Bettens, *Tetrahedron* **1974**, *30*, 1253–1260.
[45] A. B. Lovell, K. Brezinsky, I. Glassman, *Int. J. Chem. Kinet.* **1989**, *21*, 547–560.
[46] L. Zhu, J. W. Bozzelli, *J. Chem. Phys.* **2003**, *118-119*, 3696–3703.
[47] Z. F. Xu, M. C. Lin, *J. Chem. Phys.* **2006**, *124-125*, 1672–1677.
[48] J. G. Radziszewski, M. R. Nimlos, P. R. Winter, G. B. Ellison, *J. Am. Chem. Soc.* **1996**, *118*, 7400–7401.
[49] G. P. Ayers, A. D. E. Pullin, *Chem. Phys. Lett.* **1974**, *29*, 609–615.
[50] J. P. Perchard, *Chem. Phys.* **2001**, *273*, 217–233.
[51] Y. Bouteiller, J. P. Perchard, *Chem. Phys.* **2004**, *305*, 1–12.
[52] L. A. Montero, A. M. Esteva, J. Molina, A. Zapardiel, L. Hernandez, H. Marquez, A. Acosta, *J. Am. Chem. Soc.* **1998**, *120*, 12023–12033.
[53] L. A. Montero, J. Molina, J. Fabian, *Int. J. Quantum Chem.* **2000**, *79*, 8–16.
[54] M. J. S. Dewar, E. G. Zoebisch, E. F. Healy, J. J. P. Stewart, *J. Am. Chem. Soc.* **1985**, *107*, 3902–3909.
[55] J. J. P. Stewart, *J. Comput. Chem.* **1990**, *11*, 543–544.
[56] Gaussian 03, Revision E.01, M. J. Frisch, H. B. Schlegel, G. E. Scuseria, J. R. C. M. A. Robb, J. A. Montgomery, Jr., K. N. Kudin, J. M. Millam, S. S. Iyengar, J. Tomasi, B. M. V. Barone, M. Cossi, G. Scalmani, N. Rega, H. N. G. A. Petersson, M. Hada, M. Ehara, K. Toyota, J. H. R. Fukuda, M. Ishida, T. Nakajima, Y. Honda, O. Kitao, M. K. H. Nakai, X. Li, J. E. Knox, H. P. Hratchian, J. B. Cross, J. J. C. Adamo, R. Gomperts, R. E. Stratmann, O. Yazyev, R. C. A. J. Austin, C. Pomelli, J. W. Ochterski, P. Y. Ayala, G. A. V. K. Morokuma, P. Salvador, J. J. Dannenberg, S. D. V. G. Zakrzewski, A. D. Daniels, M. C. Strain, D. K. M. O. Farkas, A. D. Rabuck, K. Raghavachari, J. V. O. J. B. Foresman, Q. Cui, A. G. Baboul, S. Clifford, B. B. S. J. Cioslowski, G. Liu, A. Liashenko, P. Piskorz, R. L. M. I. Komaromi, D. J. Fox, T. Keith, M. A. Al-Laham, A. N. C. Y. Peng, M. Challacombe, P. M. W. Gill, W. C. B. Johnson, M. W. Wong, C. Gonzalez, J. A. Pople, Gaussian Inc., Pittsburgh PA, **2003**.
[57] C. T. Lee, W. T. Yang, R. G. Parr, *Phys. Rev. B* **1988**, *37*, 785–789.
[58] A. D. Becke, *J. Chem. Phys.* **1993**, *98*, 5648–5652.
[59] Y. Zhao, N. E. Schultz, D. G. Truhlar, *J. Chem. Theory Comput.* **2006**, *2*, 364–382.
[60] Y. Zhao, D. G. Truhlar, *J. Chem. Phys.* **2006**, *124-125*, 5121–5129.
[61] Y. Zhao, D. G. Truhlar, *J. Chem. Theory Comput.* **2006**, *2*, 1009–1018.
[62] Y. Zhao, D. G. Truhlar, *J. Chem. Phys.* **2006**, *124–125*, 10478–10486.
[63] R. Krishnan, J. S. Binkley, R. Seeger, J. A. Pople, *J. Chem. Phys.* **1980**, *72*, 650–654.
[64] S. F. Boys, F. Bernardi, *Mol. Phys.* **1970**, *19*, 553.
[65] G. D. Purvis, R. J. Bartlett, *J. Chem. Phys.* **1982**, *76*, 1910–1918.
[66] MOLPRO, Version 2006.1, H.-J. Werner, P. J. Knowles, R. Lindh, F. R. Manby, M. Schütz, P. Celani, T. Korona, A. Mitrushenkov, G. Rauhut, T. B. Adler, R. D. Amos, A. Bernhardsson, A. Berning, D. L. Cooper, M. J. O. Deegan, A. J. Dobbyn, F. Eckert, E. Goll, C. Hampel, G. Hetzer, T. Hrenar, G. Knizia, C. Köppl, Y. Liu, A. W. Lloyd, R. A. Mata, A. J. May, S. J. McNicholas, W. T. Meyer, M. E. Mura, A. Nicklaß, P. Palmieri, K. Pflüger, R. Pitzer, M. Reiher, U. Schumann, H. Stoll, A. J. Stone, R. Tarroni, T. Thorsteinsson, M. C. Wang, A. Wolf.
[67] C. Gonzalez, H. B. Schlegel, *J. Chem. Phys.* **1989**, *90*, 2154–2161.
[68] NBO Version 3.1, E. D. Glendening, A. E. Reed, J. E. Carpenter, F. Weinhold.

Received: December 8, 2009
Revised: June 2, 2010
Published online: July 14, 2010

